JOC The Journal of Organic Chemistry

pubs.acs.org/joc Article

Nuclear Magnetic Resonance Study of CO_2 Capture by Fluoroalkylamines: Ammonium Ion pK_a Depression via Fluorine Modification and Thermochemistry of Carbamylation

Brian Jameson, Kari Knobbe, and Rainer Glaser*

Cite This: J. Org. Chem. 2023, 88, 11534−11544 Read Online

ACCESS | Metrics & More | Article Recommendations | Supporting Information

ABSTRACT: We are developing energy-efficient and reversible carbon capture and release (CCR) systems that mimic the Lys^{201} carbamylation reaction in the active site of ribulose-1,5-bisphosphate carboxylase-oxygenase (RuBisCO). The multiequilibria scenario ammonium ion **Xa** ⇌ amine **Xb** ⇌ carbamic acid **Xc** ⇌ carbamate **Xd** requires the presence of both free amine and CO_2 for carbamylation and is affected by the pK_a(**Xa**). Two fluorination strategies aimed at ammonium ion pK_a depression and low pH carbamylation were analyzed with (2,2,2-trifluoroethyl)butylamine **2b** and 2,2-difluoropropylamine **3b** and compared to butylamine **1b**. The determination of K_1 and ΔG_1 of the carbamylation reactions requires the solution of multiequilibria systems of equations based on initial conditions, ^{1}H NMR measurements of carbamylation yields over a wide pH range, and knowledge of K_2−K_5 values. K_2 and K_3 describe carbonic acid acidity, and ammonium ion acidities K_4 were measured experimentally. We calibrated carbamic acid acidities K_5 based on the measured value K_6 of aminocarbamic acid using isodesmic reactions. The proton exchange reactions were evaluated with ab initio computations at the APFD/6-311+G* level in combination with continuum solvation models and explicit solvation. The utilities of **1**−**3** will be discussed as they pertain to the development of fluorine-modified RuBisCO-mimetic reversible CCR systems.

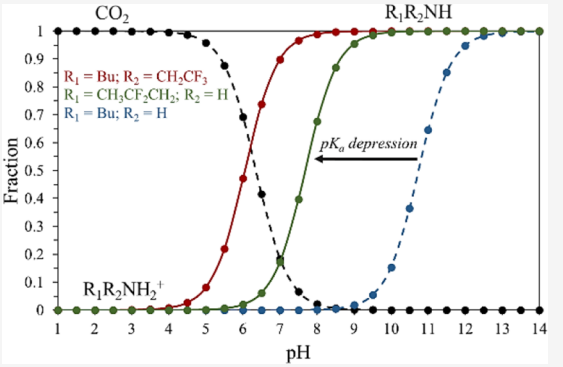

INTRODUCTION

CO_2 capture and release (CCR) systems featuring amines have been extensively studied to capture CO_2 at concentrated sources,[1−3] and recent interest is aimed at the development of materials with high amine densities for fast capture and release.[4,5] All of these materials require high energy for CO_2 release.[6] We have focused on developing biomimetic systems that feature low energy CO_2 release. Ribulose-1,5-bisphosphate carboxylase-oxygenase (RuBisCO) is a naturally occurring enzyme that is responsible for nearly all CO_2 fixation.[7−9] This enzyme is first activated by a CO_2 molecule and catalyzes the formation of 3-phospho-D-glycerate from ribulose 1,5-bisphosphate RuBP and CO_2. The active site of spinach RuBisCO features the amino acid sequence Lys^{201}-Asp^{202}-Asp^{203}-Glu^{204} where the side chain amine of Lys^{201} undergoes a low-energy reversible carbamylation reaction. The carbamate is stabilized by a Mg^{2+} ion, which is coordinated to the Asp^{203}-Glu^{204} moiety.[10−13] It is well known that both a deprotonated amine and metal cation are required for full activation of the enzyme.[14,15] Although a competing oxygenase reaction pathway and a moderate energy requirement for the H_2O/CO_2 exchange reaction complicates the carbamylation,[16,17] this activation reaction in the active site of the enzyme is of great interest for its energy-efficient reversibility.[18,19]

The KDDE sequence in the active site of RuBisCO features an octahedral complex with a Mg^{2+} ion, and it is believed to be the smallest fraction that replicates the RuBisCO active site. Yang, Schell, and Glaser recently investigated the CO_2 capture mechanism and experimentally quantified the extent of capture of the capped CH_3O-Lys-Asp-Asp-Glu-NH_2 ("KDDE") oligopeptide.[20−23] RuBisCO possesses the unique ability to depress the pK_a of the lysine side chain amine such that it becomes available as a nucleophile in pH conditions where CO_2 is present in solution. This structural feature is not retained in the capped KDDE system, and the metal precipitates from solution before deprotonation of the sidechain lysine occurs. Our approach to this problem aims at inductively lowering the pK_a of the side chain amine of lysine such that its carbamate would be formed at lower pH values. As an important pilot study to assess this approach, we quantified pK_a depression via fluorination of alkylamines.

Received: March 30, 2023
Published: August 2, 2023

https://doi.org/10.1021/acs.joc.3c00701
J. Org. Chem. 2023, 88, 11534−11544

Scheme 1. Carbamylation Pathway of Amines 1b (R_1 = Bu, R_2 = H), 2b (R_1 = Bu, R_2 = CH_2CF_3), and 3b (R_1 = $CH_3CF_2CH_2$, R_2 = H)

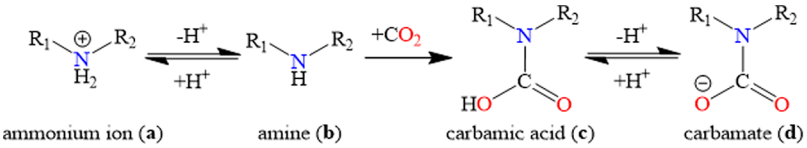

Here, we report on the results of carbamylation studies of (2,2,2-trifluoroethyl)butylamine **2b** and 2,2-difluoropropylamine **3b** (Scheme 1). These amines are excellent models to explore the effects of fluorination in carbamylation of fluorinated oligopeptides because the side chain amine in the lysine residue is the only participating functional group directly involved in CO_2 capture in both RuBisCO and the capped KDDE tetramer. It will be shown that the inductive electron withdrawal via fluorine around the amine ($-CF_2-$ *vs* $-CF_3$) may be analyzed by comparing the experimentally determined pK_a of the ammonium ions **2a** and **3a** and by comparing the efficiency of carbamylation leading to **2d** and **3d**, respectively. The extent of capture was determined by analyzing pH-dependent ^{1}H NMR spectra, and the Gibbs' free energy ΔG_{R1} of the overall carbamylation reaction $R_1R_2NH + CO_2 \rightleftharpoons R_1R_2N(COOH)$ will be determined for **2b** and **3b** by solving a system of equations that completely describe the mutiequilibria of amine carbamylation.

RESULTS AND DISCUSSION

Acidity Curves of Ammonium Ions 1a−3a and Exposition of the Problem. The pH dependencies of the acid dissociation of ammonium ions **1a−3a**, of the bicarbonate/CO_2 equilibrium, and of $Mg(OH)_2$ formation each are described by one equilibrium constant (eqs I−III). Equilibrium constants K_{CO_2} and $K_{Mg(OH)_2}$ are well known.[24−26] The acidity constants K_{amm} for reactions **Xa** ⇌ **Xb** were measured as part of the present investigation, and the evaluation of the titration curves resulted in pK_a(**1a**) = 10.74, pK_a(**2a**) = 6.05, and pK_a(**3a**) = 7.68.

It has been shown that increasing alkyl substitution increases the pK_a of ammonium ions. Rio et al. measured the pK_a of several amines including hexylamine (pK_a = 10.64), *N*-methyl-*N*-hexylamine (pK_a = 11.50), octylamine (pK_a = 10.65), and *N*-methyl-*N*-hexylamine (pK_a = 11.26).[27] It has also been shown that increasing alkyl length increases the pK_a of ammonium ions. King et al. studied several secondary amines including dimethylamine (pK_a = 10.64), diethylamine (pK_a = 10.98), dipropylamine (pK_a = 11.00), and dibutylamine (pK_a = 11.25).[28]

Productive amine carbamylation, however, is determined not only by electron density on the nitrogen, but also by steric hindrance from N-substitution. The effect of alkyl substitution (1°, 2°, 3°) in amino-functionalized CO_2 adsorbents was investigated by Ko et al.[29] They found that the maximum load capacity of 2° alkylamines was 27% lower than 1° alkylamines and that further substitution decreased load capacity by an additional 21%. Puxty et al. analyzed the CO_2 capture of several alkoxy substituted amines and found that the extent of carbamylation is highly contingent on the degree of N-substitution (1°, 2°, 3°) and the pK_a of the corresponding ammonium ion, which was altered by the position the hydroxyl group.[30]

$$R_1R_2NH_2^+ \rightleftharpoons R_1R_2NH + H^+,\ K_{amm} = \frac{[R_1R_2NH][H^+]}{[R_1R_2NH_2^+]} \quad (I)$$

$$HCO_3^- \rightleftharpoons CO_2 + OH^-,\ K_{CO_2} = \frac{[CO_2][OH^-]}{[HCO_3^-]} \quad (II)$$

$$Mg(OH)_2 \rightleftharpoons Mg^{2+} + 2OH^-,\ K_{Mg(OH)_2} = \frac{[Mg^{2+}][OH^-]^2}{[Mg(OH)_2]} \quad (III)$$

With the pK_a values of the ammonium ions **1a−3a**, we can now illustrate qualitatively the fundamental challenge of carbamylation. Productive carbamylation requires the coexistence of CO_2 and free amine, that is, high value of fractions $f(CO_2) = [CO_2]/[HCO_3^-]$ and f(**Xb**) = [**Xb**]/[**Xa**]. We show in Figure 1 the pH dependence of these fractions, which are

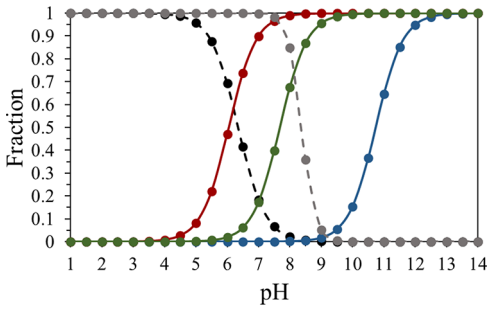

Figure 1. Fraction of CO_2 and of the amines as a function of pH in single equilibria: $f(CO_2) = [CO_2]/[HCO_3^-]$ (black pK_a = 6.352[24]), f(**1b**) = [**1b**]/[**1a**] (blue), f(**2b**) = [**2b**]/[**2a**] (red), and f(**3b**) = [**3b**]/[**3a**] (green), $f(Mg^{2+}) = [Mg^{2+}]/[Mg(OH)_2]$ (gray pK_a = 11.25[26]).

computed based on the individual equilibria of eqs I−III as opposed to the complex multiequilibrium associated with the carbamylation reaction (*vide infra*). The areas are highlighted in which the concentrations of CO_2 and free amine RNH_2 show the greatest overlap.

As can be seen from the black $f(CO_2)$ curve, the concentration of CO_2 decreases rapidly as soon as bicarbonate formation becomes significant above pH 6. The blue f(**1b**) curve shows that free butylamine coexists with CO_2 in a very narrow pH range where neither of the substrate concentrations are substantial. The situation is greatly improved for both fluorinated amines. The reduced pK_a values of the fluorinated ammonium ions **2a** and **3a** result in a much larger overlap with the CO_2 region at lower pH and with drastically higher substrate concentrations.

In Figure 1, we have also included the gray $f(Mg^{2+})$ curve because of its relevance for carbamylation of a Mg^{2+}-complexed KDDE fragment in the active site of RuBisCO. It is an added bonus of the fluorinated amine **2a** and **3a** that the $f(Mg^{2+})$

https://doi.org/10.1021/acs.joc.3c00701
J. Org. Chem. 2023, 88, 11534−11544

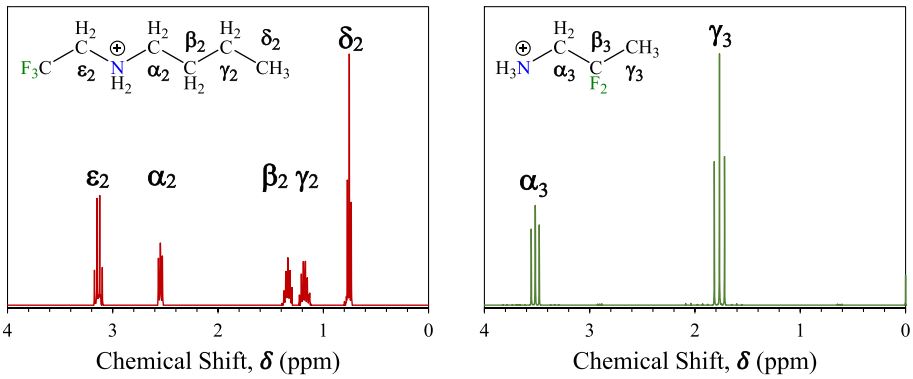

Figure 2. ^{1}H NMR spectrum of (2,2,2-trilfuoroethyl)butylammonium ion **2a** (red, left) and 2,2-difluoropropylammonium ion **3a** (green, right) in 90% H_2O:10% D_2O.

curve indicates that $Mg(OH)_2$ precipitation is not expected in the pH region of optimal carbamylation. This information suggests that carbamylation of Mg^{2+}-complexed fluorinated lysine derivatives in ^{F}KDDE is possible and probable.

NMR Analysis and Extent of Carbamylation as a Function of pH. *NMR Spectra of Ammonium Ions 1a−3a.* ^{1}H NMR spectra were acquired for ammonium ions **2a** and **3a** (Figure 2), and they are compared to those of butylammonium ion **1a**.[22] The peak labels describe the position relative to the N-atom (i.e., α, β, etc.), and the subscript denotes the corresponding ammonium ion (2,2,2-trifluoro-ethyl)-butylamine, **2**, or 2,2-difluoropropylamine, **3**. The chemical shifts for butylammonium ion **1a** were reported previously, and they are α_1 (2.52 ppm), β_1 (1.31 ppm), γ_1 (1.24 ppm), and δ_1 (0.79 ppm). A residual water peak was observed at 4.79 ppm in all spectra.

The hydrogen at the ε_2 position (3.14 ppm) for **2a** is the most deshielded due to electron withdrawal by the $-CH_2CF_3$ (tF) fluorines. The tF appendage also decreases the electron density at nitrogen and causes the α_2 (2.55 ppm) and β_2 (1.38 ppm) signals to be slightly more deshielded compared **1a** while the opposite is observed for the γ_2 (1.18 ppm) and δ_2 (0.75 ppm) signals. The H(ε_2) signal appears as a quartet with $^3J(^1H,^{19}F)$ = 9.95 Hz coupling.[31] As expected, fast exchange of the ammonium hydrogens occurs and no $^3J(^1H,^1H)$ coupling is observed for H(ε_2) and H(α_2).

The ammonium ion **3a** experiences strong inductive electron withdrawal by fluorine in its 2,2-difluoropropyl (dF) chain with H(α_3) appearing at δ = 3.68 ppm and is more deshielded than both H(α_2) and H(ε_2). Note that the fluorine di-substitution in **3a** shifts the H(α_3) signal more than fluorine tri-substitution in **2a** shifts the H(ε_2) signal. This implies that the additional fluorine in **2a** does not compensate for the −I effect of the butyl chain on the nitrogen density. The α_3 signal and the γ_3 signal at δ = 1.79 ppm both appear as $^3J(^1H,^{19}F)$ coupled triplets with 15.40 and 19.38 Hz, respectively.

NMR Monitoring of Carbamylation as a Function of pH for 2 and 3. The carbamylation reactions of **2** and **3** were monitored by acquisition of ^{1}H NMR spectra for **2** at pH values in the range 6 ≤ pH ≤ 9 (Figure 3) and for **3** at pH values between 7 ≤ pH ≤ 10 (Figure 4). In the following discussion, the term "parent signal" refers to NMR peaks that arise from the substrate (i.e., ammonium ion **Xa** ⇌ amine **Xb** equilibrium) while the term "daughter signal" refers to NMR peaks from the product (i.e., carbamic acid **Xc** ⇌ carbamate **Xd** equilibrium), the descendant of the substrate. All peaks are

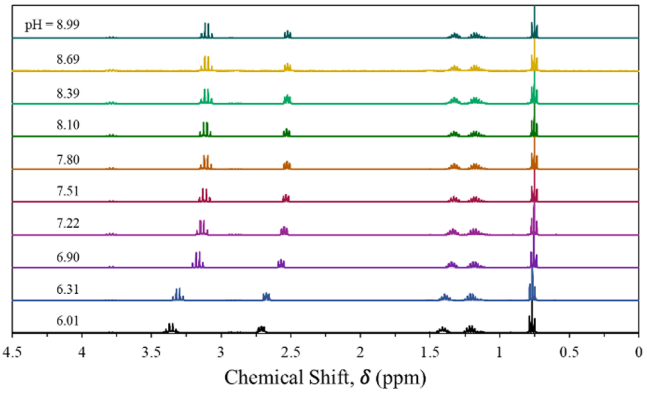

Figure 3. ^{1}HNMR spectra of **2** as a function of pH.

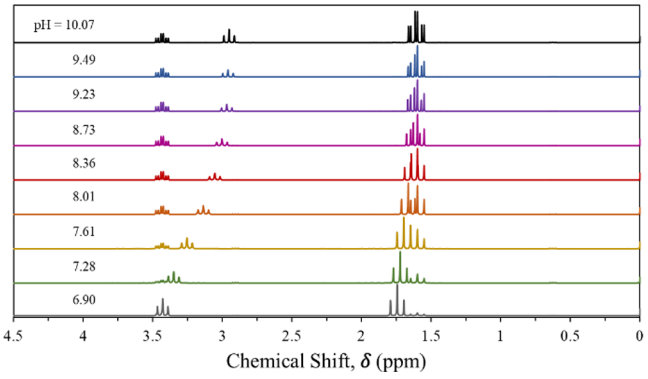

Figure 4. ^{1}HNMR spectra of **3** as a function of pH.

reported relative to an internal standard DSS signal. All pH profiles are scaled such that the most intense peak (δ_2 and γ_3) has the same magnitude in each spectrum and doing so allows for facile determination of the relative intensities between daughter and parent peaks at each pH. The measured chemical shifts, peak multiplicities, and coupling constants are reported for **2** and **3** in Tables S2 and S3, respectively.

The spectra of **2** feature one daughter peak dε_2 at about 3.8 ppm, which was confirmed by two-dimensional HSQC. This daughter signal appears as a quartet because of $^3J(^1H,^{19}F)$ coupling. Daughter peaks corresponding to the butyl chain were not discernable from the parent signals. The spectra of **3** show two discernable daughter peaks at 3.4 ppm (dα_3) and 1.6 ppm (dγ_3), which were confirmed by two-dimensional HSQC. The dα_3 daughter signal appears as a doublet of triplets. The

https://doi.org/10.1021/acs.joc.3c00701
J. Org. Chem. 2023, 88, 11534−11544

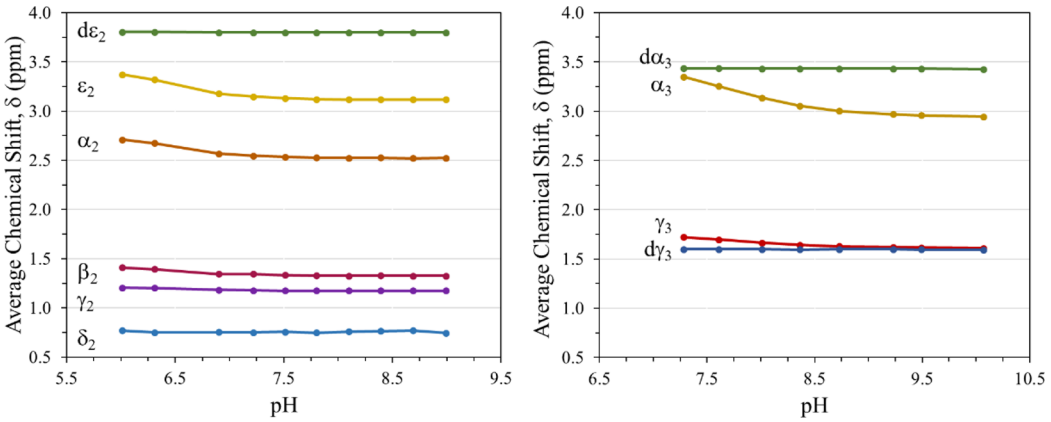

Figure 5. ^{1}H NMR chemical shift as a function of pH of **2** (left) and **3** (right).

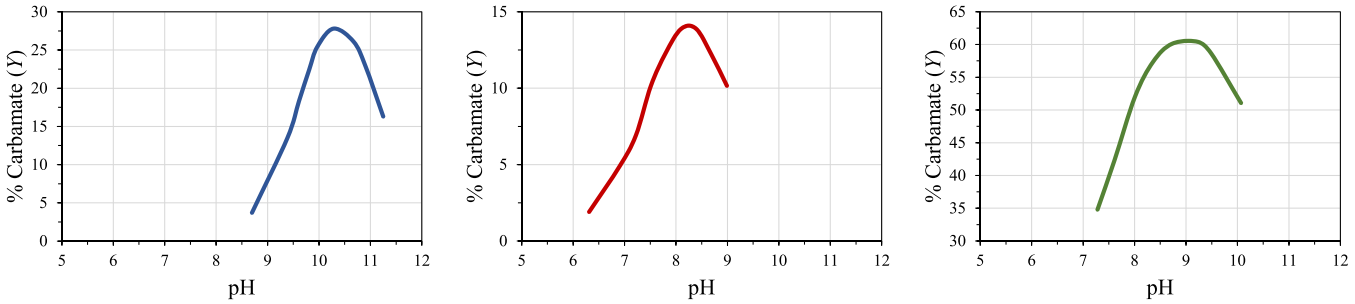

Figure 6. Carbamate mol fraction Y as a function of pH for **1** (blue, left), **2** (red, middle), and **3** (green, right).

NH hydrogen in the carbamate does not exchange and therefore provides a doublet splitting to the α_3 methylene hydrogens in addition to their triplet splitting by the CF_2 fluorines. Both the $^{3}J(^{1}H,^{19}F)$ and $^{3}J(^{1}H,^{1}H)$ coupling constants were measured and are included in Table S3. The $d\gamma_3$ daughter triplet appears well separated from its parent peak at low pH only.

Amine vs Carbamate: NMR Chemical Shifts and $^{3}J(^{1}H,^{19}F)$ Coupling Constants. The hydrogen chemical shifts of **2** and **3** are plotted in Figure 5 as a function of pH. The parent peaks correspond to the average chemical shifts resulting from the equilibria ammonium ion **Xa** ⇌ amine **Xb**, and they are greatly affected by pH as expected. Every hydrogen atom in the ammonium cation will be more deshielded compared to the neutral amine, and one thus expects the average chemical shift for all the hydrogens to decrease with increasing pH. The magnitude of this pH-dependent shift is largest for hydrogens in the proximity to the N atom, i.e., ε_2, α_2, and α_3. This feature is also observed in the parent system **1**.[22]

In contrast, the chemical shifts of the daughter signals $d\varepsilon_2$ of **2** and $d\alpha_3$ and $d\gamma_3$ of **3** are essentially constant over the entire pH range. The acid dissociation equilibrium carbamic acid **Xc** ⇌ carbamate **Xd** and the equilibrium carbamate **Xd** ⇌ zwitterion **Xe** both lie predominantly on the side of the carbamate (*vide infra*).

The chemical shifts in the high pH region of the plots in Figure 5 inform about the electron density effects of converting the amine to a carbamate. The hydrogen chemical shifts of the methylene group that carries the CF_3 group ($\varepsilon_2/d\varepsilon_2$) and the N atom are higher compared to methylene groups that carries the CF_2 group ($\alpha_3/d\alpha_3$) and the N atom, and both of these are much higher than the H-chemical shift of the methyl group ($\gamma_3/d\gamma_3$) attached only to the CF_2 group; this is as expected based on inductive effects. Note that the chemical shifts of the $d\varepsilon_2$ and $d\alpha_3$ signals are higher than for the ε_2 and α_3 signals, and this difference is due to conjugation. The nitrogen atom in the carbamate engages in negative hyperconjugation[32] and leads to a reduction of the N electron density, which propagates to the adjacent methylene groups.

The electronic difference between the amine and its carbamate also is evidenced in the $^{3}J(^{1}H,^{19}F)$ coupling constants. Figure S2 shows that the splitting of the $d\varepsilon_2$ and $d\alpha_3$ peaks is significantly lower than for the parent peaks, which is consistent with reduced CH electron density in the carbamates. The fact that $^{3}J(H\varepsilon_2,F) < {}^{3}J(H\alpha_3,F)$ shows that the methylene group in **2** starts out to be more depleted than the corresponding methylene group in **3** and additional electron depletion associated with carbamate formation is more modest; $[^{3}J(H\varepsilon_2,F) - {}^{3}J(Hd\varepsilon_2,F)] < [^{3}J(H\alpha_3,F) - {}^{3}J(Hd\alpha_3,F)]$. Carbamate formation in **3** does not exert a large effect at the methyl group γ_3, which is three σ bonds removed from the nitrogen. The $^{3}J(^{1}H,^{19}F)$ values are essentially the same for the methyl group ($\gamma_3/d\gamma_3$) of the amine and its carbamate.

Extent of Carbamate Formation of 1−3. The carbamate mol fraction Y (eq IV) measures the yield of the carbamylation reaction **Xb** + CO_2 ⇌ **Xc**. The Y values for **1**−**3** are plotted as a function of pH in Figure 6. The extent of carbamate formation was monitored by integration of the daughter signals ($d\varepsilon_2$ and $d\alpha_3$) and their corresponding parent signal integrations (ε_2 and α_3).

$$Y = \frac{[R_1R_2NCOOH] + [R_1R_2NCOO^-]}{[R_1R_2NH] + [R_1R_2NH_2^+] + [R_1R_2NCOOH] + [R_1R_2NCOO^-]} \quad \text{(IV)}$$

https://doi.org/10.1021/acs.joc.3c00701
J. Org. Chem. 2023, 88, 11534−11544

Since the parent peaks are an averaged signal arising from the equilibrium ammonium ion **Xa** ⇌ amine **Xb**, the integration of a parent peak $\int p(\mathbf{X})$ is proportional to the concentration $[p(\mathbf{X})] = [\mathbf{Xa}] + [\mathbf{Xb}]$. The daughter peaks are in a similar equilibrium; however, since the carbamate is the predominant species in this pH range (*vide infra*), the integration of the daughter peak $\int d(\mathbf{X})$ parallels the concentration $[d(\mathbf{X})] = [\mathbf{Xc}] + [\mathbf{Xd}] + [\mathbf{Xe}] \approx [\mathbf{Xd}]$. Yang et al. investigated carbamate formation as a function of pH for **1** (blue, left), a maximum carbamylation of 27.8% was observed at a pH of 10.28,[20-22] and this value provides our reference. Maximum carbamylation of **2** (middle, red) occurs at pH = 8.10 with a 13.7% capture efficiency and at pH = 9.03 for **3** (right, green) with 60.9% capture efficiency. A discussion of the interplay of *Y*, the Gibbs' free energy of carbamylation ΔG_1, and the pH of carbamylation will be discussed in greater detail (*vide infra*).

The pH values of equal substrate concentrations $f(CO_2) \approx f(R_1R_2NH)$ are about 6 ($f \approx 60\%$), 7 (20%), and 8.5 (<5%), respectively, for **2**, **3**, and **1**, respectively (Figure 1). Maximum carbamylation always occurs roughly two pH units higher than the pH of an equal substrate concentration.

Thermochemistry of Carbamylation of Amines 2b and 3b. *Multiequilibria Evaluation to Deduce* ΔG_1. We investigated the thermochemistry involved in the carbamylation of amines **2b** (R_1 = Bu, R_2 = CH_2CF_3) and **3b** (R_1 = $CH_2CF_2CH_3$, R_2 = H). The reaction of interest is the formation of a carbamic acid **Xc** from the deprotonated amine **Xb** and carbon dioxide (reaction R1). Carbamylation is complex because each species involved in reaction R1 engages in pH-dependent equilibria. To calculate the equilibrium constant K_1 and the associated Gibbs' free energy ΔG_1, a system of equations was studied involving reactions R2−R5.

A bicarbonate anion can be formed via reactions R2a and R2b, and its deprotonation is reaction R3. Carbonic acid is an intermediate in reaction R2a, but it plays no role in the overall system of equations since its deprotonation is favored in the pH region of interest (pK_a = 3.4−3.7).[24,33] In high pH conditions, it has been shown that the predominant pathway of bicarbonate formation is reaction R2b, and this is the only reaction considered here.[34]

$$R_1R_2NH + CO_2 \rightleftharpoons R_1R_2NCOOH \quad \text{(R1)}$$

$$K_1 = \frac{[R_1R_2NCOOH]}{[R_1R_2NH][CO_2]} \quad (1)$$

$$CO_2 + H_2O \rightleftharpoons H_2CO_3 \rightleftharpoons H^+ + HCO_3^- \quad \text{(R2a)}$$

$$CO_2 + OH^- \rightleftharpoons HCO_3^- \quad \text{(R2b)}$$

$$K_2 = \frac{[H^+][HCO_3^-]}{[CO_2]} \quad (2)$$

$$HCO_3^- \rightleftharpoons H^+ + CO_3^{2-} \quad \text{(R3)}$$

$$K_3 = \frac{[H^+][CO_3^{2-}]}{[HCO_3^-]} \quad (3)$$

Reaction R4 is the deprotonation reaction of the ammonium ion **2a** or **3a**, and reaction R5 is the acid disassociation reaction of carbamic acid **2c** or **3c**. The ammonium ion acidity constants pK_4 of **1a−3a** and the carbamic acid acidity constants pK_5 of **1c−3c** are all $0 < pK_a < 14$, and this is one reason why the multiequilibria analysis must deal with the concentrations of all relevant conjugate acid/base pairs explicitly.[35] Equation 6 is the mass balanced equation for the starting bicarbonate concentration $[HCO_3^-]_o$. The equilibrium bicarbonate concentration $[HCO_3^-]$ is given by eq 7, which is derived from eq 6 by incorporation of the definitions for K_2 and K_3. Solving eq 7 for $[HCO_3^-]$ will provide the equilibrium CO_2 concentration $[CO_2]$ via eq 2. The daughter/parent ratio *X* is defined by eq 8 and was determined experimentally by ^{1}H NMR spectroscopy. Note that this ratio *X* is not the same as ratio *Y* in Figure 6. The fraction *X* is defined by the ratio of the total of carbamate and carbamic acid concentrations **Xc** and **Xd** relative to the total amine and ammonium ion **Xa** and **Xb** concentrations.

$$R_1R_2NH_2^+ \rightleftharpoons R_1R_2NH + H^+ \quad \text{(R4)}$$

$$K_4 = \frac{[R_1R_2NH][H^+]}{[R_1R_2NH_2^+]} \quad (4)$$

$$R_1R_2NCOOH \rightleftharpoons R_1R_2NCOO^- + H^+ \quad \text{(R5)}$$

$$K_5 = \frac{[R_1R_2NCOO^-][H^+]}{[R_1R_2NCOOH]} \quad (5)$$

$$[HCO_3^-]_o = [HCO_3^-] + [CO_2] + [CO_3^{2-}] + [R_1R_2NCOOH] + [R_1R_2NCOO^-] \quad (6)$$

$$[HCO_3^-] = \frac{[HCO_3^-]_o - [R_1R_2NCOOH] - [R_1R_2NCOO^-]}{1 + \frac{[H^+]}{K_2} + \frac{K_3}{[H^+]}} \quad (7)$$

$$X = \frac{[R_1R_2NCOOH] + [R_1R_2NCOO^-]}{[R_1R_2NH] + [R_1R_2NH_2^+]} \quad (8)$$

Equation 9 is the mass balanced equation for the substrate amine concentration $[R_1R_2NH]_o$. By substituting this definition into eq 8, we derive eq 10, which describes the protonated and deprotonated amine concentration in terms of $[R_1R_2NH]_o$ and the ratio *X*. Equation 11 is derived by substituting eq 4 into eq 10, and this equation describes the equilibrium amine concentration $[R_1R_2NH]$ as a function of the initial substrate concentration $[R_1R_2NH]_o$ and the measured $[H^+]$ and *X* value of the carbamylation reaction. Finally, by substituting eq 5 into eq 9, we arrive at eq 12, which describes the carbamic acid concentration $[R_1R_2NCOOH]$ in terms of the carbamic acid acidity constant K_5. Knowing the concentrations $[CO_2]$, $[R_1R_2NH]$, and $[R_1R_2NCOOH]$ allows for the determination of K_1.

$$[R_1R_2NH]_o = [R_1R_2NH] + [R_1R_2NH_2^+] + [R_1R_2NCOOH] + [R_1R_2NCOO^-] \quad (9)$$

$$\frac{[R_1R_2NH]_o}{1 + X} = [R_1R_2NH] + [R_1R_2NH_2^+] \quad (10)$$

$$[R_1R_2NH] = \frac{[R_1R_2NH]_o}{(1 + X)\left(1 + \frac{[H^+]}{K_4}\right)} \quad (11)$$

https://doi.org/10.1021/acs.joc.3c00701
J. Org. Chem. 2023, 88, 11534−11544

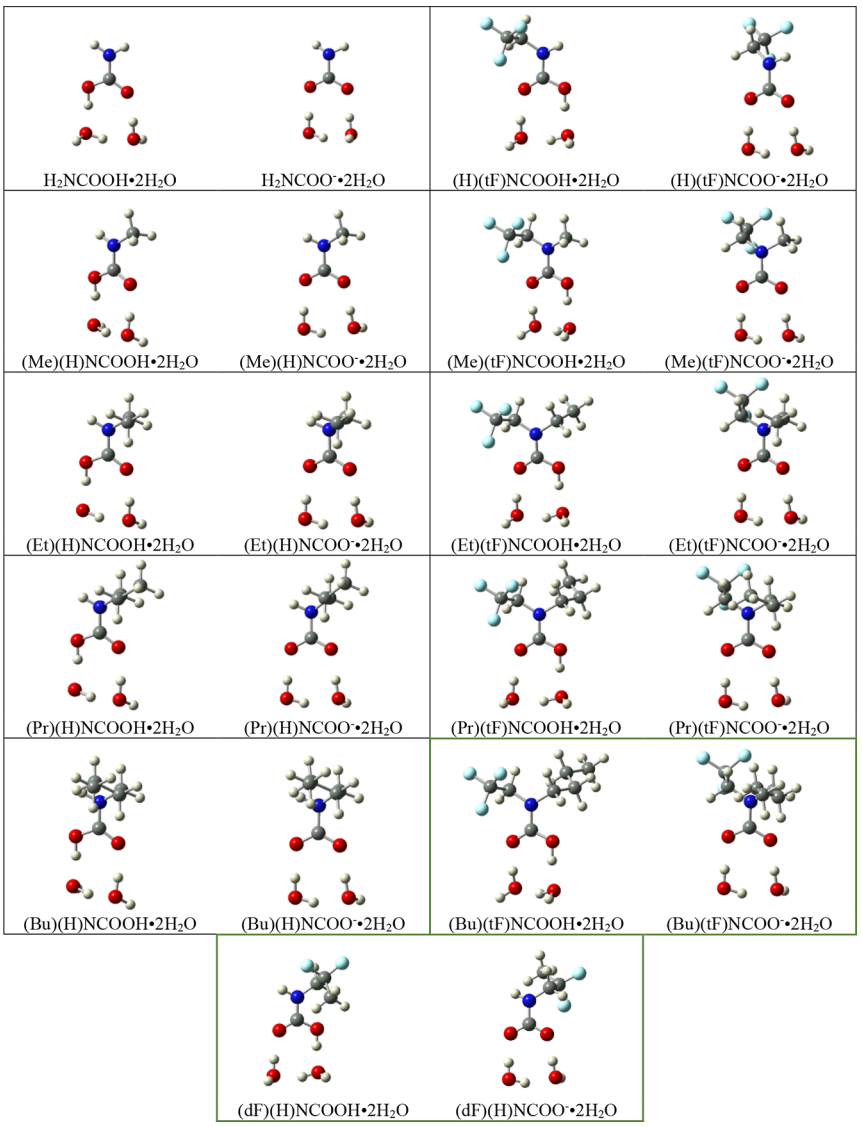

Figure 7. R_1R_2NCOOH (**Xc**) and $R_1R_2NCOO^-$ (**Xd**) models with explicit H_2O in all combinations of R_1 = H, Me, Et; R_2 = H, tF.

$$[R_1R_2NCOOH] = \frac{[R_1R_2NH]_o - [R_1R_2NH] - [R_1R_2NH_2^+]}{1 + \frac{[K_5]}{[H^+]}} \quad (12)$$

Equilibrium Constants. The equilibrium constants K_2 and K_3 of reactions R2b and R3 were reported in the literature (pK_2 = 6.352[24] or 6.18[25] and pK_3 = 10.3[36]). The acidity constants pK_4 ($R_1R_2NH_2^+ \rightleftharpoons R_1R_2NH + H^+$) were experimentally determined by strong acid/base titration (*vide supra*), and they are pK_4(**2a**) = 6.05 and pK_4(**3a**) = 7.68.

Alkyl and Fluoroalkyl Substituent Effects on Carbamic Acid Acidity. We are interested in the deprotonation reactions **Xc** ⇌ **Xd** + H^+ (reaction R5) of the N-substituted carbamic acids **2c** (R_1 = Bu; R_2 = tF) and **3c** (R_1 = dF; R_2 = H). The acidity constants K_5 for carbamic acids **2c** and **3c** are unknown, but the acidity constant K_6 was measured for the parent carbamic acid H_2NCOOH (R6; pK_6 = 5.74).[37] While the computational determination of absolute values of acidity constants remains challenging, it is much more attainable to determine accurate differences between acidities by evaluation of the isodesmic proton exchange reaction R7. The Gibbs' free energy for reaction R7 (ΔG_7) is equal to the difference $\Delta\Delta G$ between the acid dissociation reactions R5 and R6. The Gibbs' free energy ΔG_7 together with the pK_6 value allows for the determination of the desired pK_5 values (eqs 13 and 14).

$$H_2NCOOH \rightleftharpoons H_2NCOO^- + H^+ \quad (R6)$$

$$R_1R_2NCOOH + H_2NCOO^- \rightleftharpoons R_1R_2NCOO^- + H_2NCOOH \quad (R7)$$

$$\Delta G_5 = \Delta G_6 + \Delta G_7 = -RT\ln(K_6) + \Delta G_7 \quad (13)$$

$$K_5 = K_6 \bullet e^{(-\Delta G_7/RT)} \quad (14)$$

To evaluate eq 14, we determined the energies of the parent carbamic acid and its carbamate, H_2NCOOH and H_2NCOO^-, and of the alkyl substituted carbamic acids and their carbamates, R_1R_2NCOOH and $R_1R_2NCOO^-$. Accurately accounting for solvation effects on acid dissociation equilibria requires satisfactory description of specific solvation of the acid and its conjugate base. The most difficult problem is the estimation of solvation effects and questions concerning the

https://doi.org/10.1021/acs.joc.3c00701
J. Org. Chem. 2023, 88, 11534−11544

size of the water cluster models and the extrapolation to bulk solvation.[38] The solvation energy of the hydronium ion $\Delta H_{sol}(H_3O^+)$ relies on the solvation energy of the gas phase proton $\Delta H_{sol}(H^+)$, the heat of vaporization of water $\Delta H_{vap}(H_2O)$, and the proton affinity of water in the gas-phase $PA(H_2O)$.[39,40] The computation of $\Delta H_{sol}(H_3O^+)$ is based on data measured or computed[41,42] for a limited number of water clusters $H_3O^+(H_2O)_n$ and an extrapolation method to bulk solution, $H_3O^+(H_2O)_\infty$.

The isodesmic reaction R7 avoids the question of hydronium ion solvation; however, specific solvation of carbamic acids and their carbamates remains important. All models were optimized with bulk SMD solvation, and explicit solvation was explored by the addition of two water molecules ($\cdot 2H_2O$) around the carbamic acid and its carbamate.

Two basis sets were employed. Approach A utilizes the 6-311G* basis set for all species; carbamic acid, carbamate, and explicit water. Since the carbamates are anions, it is very reasonable to consider the application of the diffuse-function augmented 6-311+G* basis set. However, it has been our experience that 6-311+G* basis set is not useful for the description of the specific solvent molecules because it invites basis set superposition errors.[43,44] The diffuse functions placed on neutral solvent water molecules would contribute artificially to the description of the electron density of the carbamate. Therefore, in our approach B, we applied the 6-311+G* basis set only to the carbamic acids and their carbamates, while describing the explicit water molecules with the 6-311G* basis set. For brevity, we refer to the mixed basis set as 6-311(+)G*. Structures optimized at the SMD[APFD/6-311(+)G*] level with explicit solvation are shown in Figure 7. Thermochemical data are documented in Table S1, and Cartesian coordinates of all optimized structures are provided in the Supporting Information. The reaction energies of reaction R7 are given in Table S1 along with the derived pK_5 values.

Both basis sets (approach A *vs* approach B) and solvation methods (SMD *vs* SMD[$\cdot 2H_2O$]) were explored in all combinations for reaction R8 using the carbamic acid R_1 = Me, R_2 = H, tF (Table 1). One would expect the addition of a fluorinated substituent to decrease the acidity constant of a carbamic acid due to the I− effect of fluorine, indicated by a negative ΔG_7. Similarly, the addition of non-functionalized alkyl groups would increase the acidity constant of carbamic acids due to their I+ nature, indicated by a positive ΔG_7. This is not observed for approach A with bulk solvation. The addition of R_1 = Me yielded ΔG_7 = −0.5 kcal/mol, the addition of R_2 = tF yielded ΔG_7 = −3.7 kcal/mol, and adding both groups R_1 = Me and R_2 = tF yielded ΔG_7 = −4.1 kcal/mol. A positive ΔG_7 for alkyl addition was also not observed using approach A with explicit solvation. The addition of R_1 = Me yielded ΔG_7 = −0.2 kcal/mol, the addition of R_2 = tF yielded ΔG_7 = −2.8 kcal/mol, and adding both groups R_1 = Me and R_2 = tF yielded ΔG_7 = −2.8 kcal/mol. Approach B with explicit solvation was the only basis set/solvation combination that yielded both a positive ΔG_7 for R_1 = Me (ΔG_7 = 0.09 kcal/mol) and a negative ΔG_7 for R_2 = tF (ΔG_7 = −2.0 kcal/mol). Additionally, optimization of structures in R7 using approach B with explicit solvation yielded the lowest energy geometries.

Approach B with explicit solvation was utilized to explore reaction R7 for the much larger array of R_1 = Me, Et, Pr, Bu in all combinations with R_2 = H, tF. Increasing the alkyl length R_1 increases ΔG_7 but plateaus in magnitude as alkyl length increases. The addition of the trifluoroethyl group reduced ΔG_7 in all combinations with all R_1 substitutions. We obtained a calibrated pK_5(**2c**) = 5.85 by adding R_1 = Bu and R_2 = tF and pK_5(**3c**) = 5.65 by adding R_1 = dF and R_2 = H. Although these values are not vastly different in magnitude from the parent carbamic acid (pK_6 = 5.74), their effects in the much larger system of equations are not negligible.

Table 1. Reaction Thermochemistry Data for R7 Calculated at APFD Comparing the Effect of Adding Alkyl and Trifluoroethyl Substituents[a]

solv. model	basis set	R_1	R_2	ΔG_7	$T\cdot\Delta S_7$	pK_5
SMD bulk solvation	A	Me	H	−0.51	0.02	5.37
		H	tF	−3.68	0.75	3.04
		Me	tF	−4.05	0.64	2.77
SMD bulk solvation + explicit water		Me	H	−0.19	−0.04	5.60
	A	H	tF	−2.84	0.20	3.76
		Me	tF	−2.84	0.54	3.66
		Me	H	0.09	0.57	5.81
	B	H	tF	−1.99	0.20	4.28
		Me	tF	−1.29	0.25	4.79
SMD bulk solvation + explicit water	B	Me	H	0.09	0.62	5.81
		Et	H	0.41	0.36	6.04
		Pr	H	0.65	0.13	6.22
		Bu	H	0.64	0.07	6.21
	B	Me	tF	−1.29	0.27	4.79
		Et	tF	−1.04	0.37	4.98
		Pr	tF	−0.70	0.44	5.23
		Bu	tF	0.15	0.89	5.85
	B	dF	H	−0.12	−0.10	5.65

[a]Approach A: SMD[APFD/6-311G*]; Approach B: SMD[APFD/6-311(+)G*].

*Reaction Energy $\Delta G_1°$ of Carbamylation for Amines **2** and **3**.* The Gibbs' free energy ΔG_1 for the overall carbamylation reaction R1 was calculated using the definition for the equilibrium constant of carbamylation K_1 (eq 1). The determination of K_1 is difficult because of the pH dependencies of the concentrations of the substrates [CO_2] and [R_1R_2NH] and of the product [$R_1R_2NHCOOH$] and requires the knowledge of the daughter/parent ratio X, the initial concentrations $[HCO_3^-]_o$ and $[R_1R_2NH_2]_o$, and analysis of the multiequilibria (eqs 2−12) of all species involved in R1 at discreet pH values (Tables 2 and 2). The amine concentration [R_1R_2NH] depends only on the ratio X and K_4 (eq 11). In Tables 2 and 3, two concentrations of CO_2 are listed based on the two literature values of K_2 employed in eq 2. The carbamate concentration [$R_1R_2NHCOO^-$] and the carbamic acid concentration [$R_1R_2NHCOOH$] were calculated using both the pK_5 value of the parent carbamic acid and with our best estimates of pK_5 for the substituted systems. The precise value of pK_5 does not affect these concentrations significantly but it does affect the multiequilibria indirectly in other ways.

We calculated ΔG_1 as a 2 × 2 matrix employing either one of the two literature values of pK_2 and using either the pK_5 of the parent carbamic acid (R_1 = R_2 = H) or the calibrated pK_5 with R_1, R_2 substitutions. The resulting four sets **i**−**iv** of ΔG_1 values are listed in Tables 2 and 3, and the ΔG_1 values are plotted in Figure 8 as a function of pH. The ΔG_1 values for **2** are shown in yellow (pK_5 = 5.74) and green (pK_5 = 5.85), and they are shown for **3** in red (pK_5 = 5.74) and blue (pK_5 = 5.65). Depending on the acidity constant K_2, ΔG_1 values are shown

https://doi.org/10.1021/acs.joc.3c00701
J. Org. Chem. 2023, 88, 11534−11544

Table 2. Measured Daughter/Parent Ratio, Calculated Concentrations, and Derived ΔG_1 for Carbamylation of 2[a,b,c,d]

pH	X (%)	$[R_1R_2NH]$	$[R_1R_2NCO_2H]$	$[R_1R_2NCO_2^-]$	$[CO_2]$[e]	$[CO_2]$[f]	i[e,g] ΔG_1	ii[e,h] ΔG_1	iii[f,g] ΔG_1	iv[f,h] ΔG_1
8.99	10.2	0.0452	0.0033	4.5943	0.0683	0.0460	−0.04	0.11	−0.28	−0.13
8.69	12.5	0.0442	0.0080	5.5101	0.1619	0.1090	−0.06	0.09	−0.30	−0.15
8.39	13.6	0.0437	0.0171	5.9442	0.3431	0.2309	−0.08	0.07	−0.31	−0.16
8.10	13.7	0.0434	0.0336	5.9780	0.6628	0.4461	−0.09	0.06	−0.33	−0.18
7.80	12.4	0.0436	0.0609	5.4245	1.1847	0.7972	−0.10	0.05	−0.33	−0.18
7.51	10.0	0.0438	0.0973	4.4495	1.8450	1.2417	−0.11	0.04	−0.35	−0.20
7.22	6.9	0.0436	0.1322	3.0999	2.5121	1.6906	−0.11	0.03	−0.35	−0.20
6.90	4.5	0.0418	0.1755	1.9687	3.5631	2.3979	−0.10	0.04	−0.33	−0.19

[a]R_1 = Bu, R_2 = tF. [b]$[HCO_3]_o$ = 35 mM, $[R_1R_2NH_2]_o$ = 50 mM. [c]Concentrations in mM. Energy in kcal/mol. [d]The peaks used to determine X were ε and dε. [e]Using pK_2 = 6.352.[24] [f]Using pK_2 = 6.18.[25] [g]Using pK_S = 5.85. [h]Using pK_S = 5.74.[40]

Table 3. Measured Daughter/Parent Ratio, Calculated Concentrations, and Derived ΔG_1 for Carbamylation of 3[a,b,c,d]

pH	X (%)	$[R_1R_2NH]$	$[R_1R_2NCO_2H]$	$[R_1R_2NCO_2^-]$	$[CO_2]$[e]	$[CO_2]$[f]	i[e,g] ΔG_1	ii[e,h] ΔG_1	iii[f,g] ΔG_1	iv[f,h] ΔG_1
10.07	94.7	0.1108	0.0028	72.9559	0.0018	0.0012	−1.77	−1.89	−2.01	−2.13
9.49	137.9	0.1038	0.0126	86.9302	0.0097	0.0065	−1.80	−1.92	−2.03	−2.16
9.23	150.8	0.0959	0.0237	90.1687	0.0195	0.0132	−1.80	−1.92	−2.03	−2.16
9.03	156.0	0.0561	0.0381	91.3674	0.0320	0.0216	−1.81	−1.93	−2.04	−2.17
8.73	150.7	0.0875	0.0749	90.0932	0.0651	0.0438	−1.80	−1.92	−2.04	−2.16
8.36	134.5	0.0775	0.1674	85.8670	0.1535	0.1033	−1.79	−1.91	−2.03	−2.15
8.01	108.6	0.0638	0.3394	77.7425	0.3405	0.2291	−1.78	−1.91	−2.02	−2.14
7.61	73.3	0.0437	0.6883	62.7724	0.8648	0.5820	−1.77	−1.90	−2.01	−2.13
7.28	53.3	0.0287	1.1952	50.9857	2.1773	1.4653	−1.77	−1.88	−2.00	−2.12

[a]R_1 = dF, R_2 = H. [b]$[HCO_3]_o$ = 94 mM, $[R_1R_2NH_2]_o$ = 150 mM. [c]Concentrations in mM. Energy in kcal/mol. [d]The peaks used to determine X were ε and dε. [e]Using pK_2 = 6.352.[24] [f]Using pK_2 = 6.18.[25] [g]Using pK_S = 5.65. [h]Using pK_S = 5.74.[40]

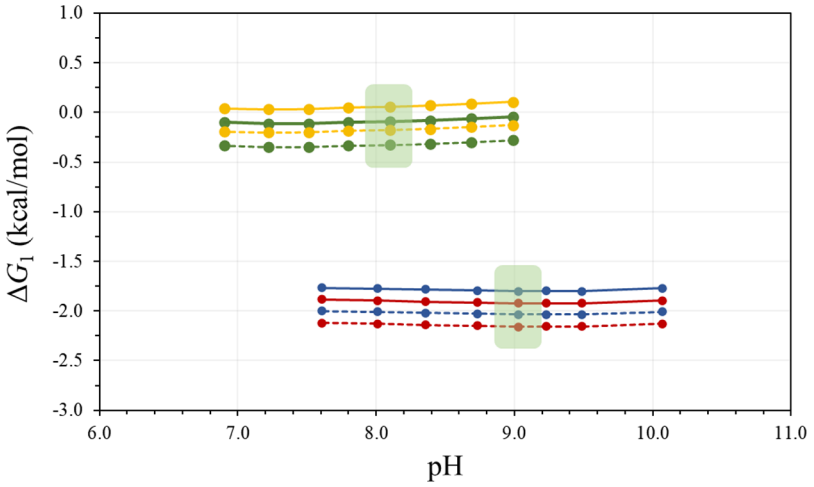

Figure 8. ΔG_1 of carbamylation for (2,2,2-trifluoroethyl)butylamine (**2**, green/yellow) and 2,2-difluoropropylamine (**3**, blue/red) as a function of pH.

with dashed lines (pK_2 = 6.18) or solid lines (pK_2 = 6.352). The green shaded areas of Figure 8 indicate the pH regions with the largest carbamate mol fractions Y (Figure 6). The measurements in those regions afford the most accurate ΔG_1 because of minimization of error associated with the integration of the parent and daughter NMR signals and are based on the measurements at pH = 8.11 and pH = 9.03 for **2** and **3**, respectively. In our judgment, the value reported by Gibbons *et al.*[24] (pK_2 = 6.352) is the better literature value. With this value and the (R_1,R_2)-calibrated values of pK_S(**2**) = 5.85 and pK_S(**3**) = 5.65, we determined the Gibbs' free energies of carbamylation ΔG_1(**2**) = −0.09 kcal/mol and ΔG_1(**3**) = −1.81 kcal/mol.

The ΔG_1(**1**) = −1.57 kcal/mol value[20-22] for the carbamylation of butylamine **1** falls between the respective value of the fluorinated amines ΔG_1(**3**) < ΔG_1(**1**) < ΔG_1(**2**). The utility of each fluorine modification depends on ΔG_1, the yield of carbamylation quantified by the carbamate mol fraction Y(**3**) > Y(**1**) > Y(**2**), and the pH at which maximum carbamylation occurs. If one were to choose a CCR system based solely on the yield of carbamylation, the clear choice is **3** given that the extent of capture for **3** is much larger than for **1**, Y(**3**) = 2.2 × Y(**1**).

CONCLUSIONS

Ammonium ion pK_a depression and amine carbamylation were quantified for butylamine **1b**, (2,2,2-trifluoro-ethyl)butylamine

https://doi.org/10.1021/acs.joc.3c00701
J. Org. Chem. 2023, 88, 11534−11544

2b, and 2,2-difluoropropylamine **3b**. The pK_a values of the ammonium ions **1a**−**3a** were determined experimentally by titration, and it was found that both fluorinated species feature lower pK_as than the parent system, i.e., pK_a(**1a**) =10.74, pK_a(**2a**) = 6.05, and pK_a(**3a**) = 7.68. The extent of carbamylation was explored as a function of pH for **2** and **3** by ^{1}H NMR spectroscopy. The spectra of **2** feature one carbamate daughter peak at 3.8 ppm (dε_2), and the spectra for **3** feature two carbamate daughter peaks at 3.4 ppm (dα_3) and 1.6 ppm (dγ_3). The extent of carbamylation was quantified with the carbamate mol fraction Y using the integrations of the daughter signals and their corresponding parent signals. Maximum carbamylation occurs at pH = 8.11 for **2** with 13.7% capture efficiency and at pH = 9.03 for **3** with 60.7% capture efficiency. Both pH values are markedly below the respective value for butylamine **1**, and this finding confirms that both fluorination strategies successfully depress ammonium ion pK_a and thereby allows for carbamylation at lower pH.

While the knowledge of the carbamate mol fraction $Y = f(R_1R_2NH,pH)$ suffices to optimize CCR systems, we went one step further and determined the Gibbs free energy ΔG_1 of the overall carbamylation reaction $R_1R_2NH + CO_2 \rightleftharpoons R_1R_2N\text{-}(COOH)$ for **2** (R_1 = Bu, R_2 = tF) and **3** (R_1 = dF, R_2 = H). This process requires the solution of a system of equations describing the multiequilibrium and relies on initial conditions as well as a set of equilibrium constants K_1−K_5. Equilibrium constants K_5(**2c**) and K_5(**3c**) describe carbamic acid acidity **Xc** ⇌ **Xd** + H^+ (R5) and were determined based on the known constant K_6 describing the aminocarbamic acid acidity $H_2N(COOH) \rightleftharpoons H_2N(COO^-) + H^+$ (R6) and computational evaluations of the isodesmic proton exchange reactions **Xc** + $H_2NCOOH \rightleftharpoons$ **Xd** + H_2NCOO^- (R7). Several theoretical models with various degrees of explicit solvation were tested, and our best estimates are pK_5(**2c**) = 5.85 and pK_5(**3c**) = 5.65. Evaluating the system of equations with the calibrated K_5(**2c**) and K_5(**3c**) constants yielded Gibbs free energies of ΔG_1(**2**) = −0.09 kcal/mol and ΔG_1(**3**) = −1.81 kcal/mol, respectively. The best estimate of the acidity constant pK_5(**1c**) = 5.89 yielded ΔG_1(**1**) = −1.57 kcal/mol.[20−22] The ΔG_1 values of **2** and **3** show that both amines are capable of reversible CO_2 capture from air.

With a view to embedding fluorinated lysines in place of lysine in the tetrapeptide KDDE, the pH value of maximum carbamylation becomes a critical parameter and our efforts aim to reduce the pH of effective capture. From this perspective, the *N*-trifluoroethyl system **2** is the more interesting one because maximum capture occurs at a pH that is a full two units lower than for **1**. Fluorinated **2** is expected to allow studies of the carbamylation reaction of metal-complexed oligopeptides, and this advantage easily outweighs the lower load capacity. We have recently published the synthesis of N^ε-(2,2,2-trifluoroethyl)lysine (^{tF}K),[45] and we have successfully embedded the unnatural lysine in the tetrapeptide ^{tF}KDDE.[46] We are currently developing methods for the syntheses of 5,5-difluorolysine and ^{dF}KDDE.

COMPUTATIONAL METHODS

Calibration of models used to determine the Gibbs' free energy ΔG_{R1} of the overall carbamylation reaction $R_1R_2NH + CO_2 \rightleftharpoons R_1R_2N\text{-}(COOH)$ relied on the evaluation of isodesmic reactions using density functional theory (DFT). The Austin−Frisch−Petersson functional with dispersion (APFD) was employed.[47] This functional was used to reduce long-range attractive and repulsive interactions and to draw direct correlation with previous work performed on butylamine **1b**.[48] The triple-zeta basis set 6-311G basis set was augmented with polarization functions on heavy atoms, 6-311G*. In a few calculations, diffuse functions were also added on heavy atoms, 6-311+G*.[49] A universal solvation model based on solute electron density (SMD) was applied to reproduce bulk aqueous solution conditions in the experimental ^{1}H NMR spectra.[50]

All structures were completely optimized, and vibrational frequencies were computed at the SMD(APFD/6-311G*) and/or SMD(APFD/6-311+G*) levels to obtain thermodynamic parameters (*vide infra*). The thermodynamic parameters were evaluated at room temperature T = 298.15 K. Cartesian coordinates of all stationary structures are provided in the Supporting Information. Computational analysis was performed with Gaussian16 on the Missouri University of Science and Technology high-performance computational cluster.[51]

The Gibbs free energy for the formation of the carbamic acid $R_1R_2NH + CO_2 \rightleftharpoons R_1R_2NCOOH$ was determined via the Gibbs equation $\Delta G_1 = -RT\cdot\ln(K_1)$ with R = 1.9872036 × 10^{-3} kcal·mol^{-1}·K^{-1} at T = 298.15 K. The constant K_1 was determined by solving the complex system of equations and employing the known acidity constants K_2 and K_3 and the acidity constants K_4 that we measured. Bulk solvation and explicit solvation were included in computational models used to estimate K_5 as described in the section "Alkyl and Fluoroalkyl Substituent Effects on Carbamic Acid Acidity."

EXPERIMENTAL METHODS

Measurements of Ammonium Ion Acidity. The experimental acidity constants (pK_4, $R_1R_2NH_2^+ \rightleftharpoons R_1R_2NH + H^+$) for ammonium ions (2,2,2-trifluoroethyl)butylamine **2a** and 2,2-difluoropropamine **3a** were determined by strong acid/base titration. A 0.1 M NaOH solution was prepared by combining 0.5 g of solid NaOH with 100 mL of distilled water. A 0.1 M solution of **2a** was prepared by mixing 1.0 g of (2,2,2-trifluoroethyl)butylamine hydrochloride with 59 mL of distilled water. Similarly, a 0.1 M stock solution of **3a** was prepared by combining 1.0 g (7.6 mmol) of 2,2-difluoropropamine hydrochloride with 76 mL of distilled H_2O. A Fisher Scientific Accumet AP110 pH/ORP meter was calibrated and placed in 20 mL of each fluorinated stock solution with a stir bar. The NaOH solution was added in small increments, recording the pH after each addition. Small volumes were used near the equivalency point to ensure a sharp change in pH. The titration curves for ammonium ions **1a**−**3a** are shown in Figure S1.

Measurements of the pH Profiles of the Carbamylation of Amines 2b and 3b. A stock solution of **2b** was generated by combining 1.1 g (5.60 mmol) of (2,2,2-trifluoroethyl)butylamine hydrochloride with 199.1 mL of 90% H_2O:10% D_2O solution and stirred until the solid dissolved completely. To this solution, 0.65 g (7.74 mmol) of sodium bicarbonate and 15.1 mg of sodium trimethylsilylpropanesulfonate (DSS) were added to generate the bulk solution. The pH of the solution was monitored by a Fisher Scientific Accumet AP110 pH/ORP meter. The pH of the bulk solution before adjustments was 3.47. The bulk solution was portioned into 10 scintillation vials each containing 20 mL of solution. The pH of each vial was adjusted with small portions of 3 M H_2SO_4 and 1 M NaOH to the desired pH. Small volumes were used to retain the original concentration of **2b**. These samples were allowed to equilibrate over a period of 48 h without venting, periodically adjusting the pH with the aforementioned acid−base solutions. Once equilibrated, ^{1}H NMR spectra were acquired for each sample.

A stock solution of **3b** was generated by combining 2.0 g of 2,2-difluoropropamine hydrochloride (15.2 mmol) with 200 mL of 10% D_2O:90% H_2O. The initial pH of the stock solution was 6.90. To the stock solution, 1.9 g of Na_2CO_3 (1.5 mol equiv) was combined with 50.5 mg of DSS. The stock solution was portioned out into 10 vials labeled 1−10, and the pH of each sample was adjusted with 3 M H_2SO_4 and 1 M NaOH. The samples were sealed and allowed to equilibrate overnight. Small adjustments with the HCl/NaOH solutions were applied till no change in pH was observed after an additional 48 h.

https://doi.org/10.1021/acs.joc.3c00701
J. Org. Chem. 2023, 88, 11534−11544

NMR Measurements with Water Suppression. Spectra were acquired using a Bruker 400 MHz Avance III HD Liquid-State NMR spectrometer. Water suppression techniques were applied using the Bruker pulse program "noesygppr1d".[52] This pulse program was chosen for pre-saturation during relaxation delay. Small sample volumes (0.5 mL) were implemented to ensure a well-suppressed water signal, along with pulse calibration and 3D shimming to remove possible gradience and improve initial homogeneity.[53]

■ ASSOCIATED CONTENT

Data Availability Statement

The data underlying this study are available in the published article and its Supporting Information.

Supporting Information

The Supporting Information is available free of charge at https://pubs.acs.org/doi/10.1021/acs.joc.3c00701.

Strong acid/base titration curves for ammonium ions **1a**−**3a**; table documenting total energies computed with two basis sets A and B in all combinations with explicit solvation; Cartesian coordinates of all stationary structures involved in reaction R7 (R_1 = Me, Et, Pr, Bu; R_2 = H, tF and R_1 = dF; R_2 = H) (PDF)

■ AUTHOR INFORMATION

Corresponding Author

Rainer Glaser − *Department of Chemistry, Missouri University of Science and Technology, Rolla, Missouri 65401, United States;* orcid.org/0000-0003-3673-3858; Email: glaserr@umsystem.edu

Authors

Brian Jameson − *Department of Chemistry, Missouri University of Science and Technology, Rolla, Missouri 65401, United States;* orcid.org/0000-0003-2872-3967

Kari Knobbe − *Department of Chemistry, Missouri University of Science and Technology, Rolla, Missouri 65401, United States;* orcid.org/0000-0002-7054-7349

Complete contact information is available at: https://pubs.acs.org/10.1021/acs.joc.3c00701

Notes

The authors declare no competing financial interest.

■ ACKNOWLEDGMENTS

The high-performance computing cluster was purchased in part with MRI funding by the National Science Foundation under Grant No. OAC-191978. This work was supported by Grant No. 1665487 from the National Science Foundation. KK gratefully acknowledges support from the Opportunities for Undergraduate Research Experiences (OURE) program. We appreciate the thoughtful and constructive comments by the reviewers.

■ REFERENCES

(1) Rochelle, G. T. Amine Scrubbing for CO_2 Capture. *Science* **2009**, *325*, 1652−1654.

(2) Wang, M.; Wei, S.; Wu, Z.; Zhou, S.; Wang, Z.; Wang, J.; Lu, X. Alkyl amine functionalized triphenylamine-based covalent organic frameworks for high-efficiency CO_2 capture and separation over N_2. *Mater. Lett.* **2018**, *230*, 28−31.

(3) Xiao, M.; Liu, H.; Gao, H.; Olson, W.; Liang, Z. CO_2 capture with hybrid absorbents of low viscosity imidazolium-based ionic liquids and amine. *Appl. Energy* **2019**, *235*, 311−319.

(4) Sarazen, M. L.; Jones, C. W. Insights into Azetidine Polymerization for the Preparation of Poly(propylenimine)-Based CO_2 Adsorbents. *Macromolecules* **2017**, *50*, 9135−9143.

(5) Pang, S. H.; Lee, L.-C.; Sakwa-Novak, M. A.; Lively, R. P.; Jones, C. W. Design of Aminopolymer Structure to Enhance Performance and Stability of CO_2 Sorbents: Poly(propylenimine) vs Poly(ethylenimine). *J. Am. Chem. Soc.* **2017**, *139*, 3627−3630.

(6) Bains, P.; Psarras, P.; Wilcox, J. CO_2 capture from the industry sector. *Prog. Energy Combust. Sci.* **2017**, *63*, 146−172.

(7) Phillips, R.; Milo, R. A feeling for the numbers in biology. *Proc. Natl. Acad. Sci.* **2009**, *106*, 21465−21471.

(8) Shively, J. M.; van Keulen, G.; Meijer, W. G. Something from almost nothing: carbon dioxide fixation in chemoautotrophs. *Annu. Rev. Microbiol.* **1998**, *52*, 191−230.

(9) Kusian, B.; Bowien, B. Organization and regulation of *cbb* CO_2 assimilation genes in autotrophic bacteria. *FEMS Microbiol. Rev.* **1997**, *21*, 135−155.

(10) Glaser, R.; Castello-Blindt, P. O.; Yin, J. Biomimetic Approaches to Reversible CO_2 Capture From Air. *N*-Methylcarbaminic Acid Formation in Rubisco-Inspired Models. Chapter 17 in *New and Future Developments in Catalysis. Activation of Carbon Dioxide*, Steven L., Suib (Ed.), 1st ed., Elsevier Publishers: August 2013, 501−534.

(11) Muelleman, A.; Schell, J.; Glazer, S.; Glaser, R. Thermochemistry of a Biomimetic and Rubisco-Inspired CO_2 Capture System from Air. *C* **2016**, *2*, 18.

(12) Hartman, F. C.; Stringer, C. D.; Milanez, S.; Lee, E. H. The active site of Rubisco. *Philos. Trans. R. Soc. London, Ser. B* **1986**, *313*, 379−395.

(13) Tayler, T. C.; Andersson, I. Multiple catalytic roles of His 287 of Rhodospirillum rubrum ribulose 1,5-bisphosphate carboxylase/oxygenase. *Biochemistry* **1997**, *36*, 4041−4046.

(14) Lorimer, G. H.; Miziorko, H. M. Carbamate formation on the .epsilon.-amino group of a lysyl residue as the basis for the activation of ribulosebisphosphate carboxylase by Carbon dioxide and Magnesium(2+). *Biochemistry* **1980**, *19*, 5321−5328.

(15) Lorimer, G. H.; Badger, M. R.; Andrews, T. J. The activation of ribulose-1,5-bisphosphate carboxylase by carbon dioxide and magnesium ions. Equilibria, kinetics, a suggested mechanism, and physiological implications. *Biochemistry* **1976**, *15*, 529−536.

(16) Bathellier, C.; Yu, L. J.; Farquhar, G. D.; Coote, M. L.; Lorimer, G. H.; Tcherkez, G. Ribulose 1,5-bisphosphate carboxylase/oxygenase activates O_2 by electron transfer. *Proc. Natl. Acad. Sci.* **2020**, *117*, 24234−24242.

(17) Glaser, R. *Advances in CO2 Capture, Sequestration and Conversion* ACS Books: Washington DC, 2015, 266−293, DOI: 10.1021/bk-2015-1194.fw001.

(18) Feller, U.; Crafts-Brander, S.; Salvucci, M. Relationship between the Heat Tolerance of Photosynthesis and the Thermal Stability of Rubisco Activase in Plants from Contrasting Thermal Environments. *Plant Physiol.* **1998**, *116*, 539−546.

(19) Chen, J.; Wang, P.; Mi, H.-L.; Chen, G.-Y.; Xu, D.-Q. Reversible association of ribulose-1, 5-bisphosphate carboxylase/oxygenase activase with the thylakoid membrane depends upon the ATP level and pH in rice without heat stress. *J. Exp. Bot.* **2010**, *61*, 2939−2950.

(20) Schell, J. *Investigation of CO2 capture systems, Lewis acid-base pairs, and oscillating reactions with electronic structure theory and kinetics-based approaches*. Ph.D. Dissertation, University of Missouri: Columbia, MO, 2020, DOI: 10.32469/10355/86509.

(21) Yang, K. *Experimental and Theoretical Studies of CO2 Capture from Air and of Crystalline, Ferroelectric, Non-Linear Optical Materials*, Ph.D. Dissertation, University of Missouri: Columbia, MO, 2022, DOI: 10.32469/10355/94102.

(22) Yang, K.; Schell, J.; Gallazzi, F.; Wycoff, W.; Glaser, R. NMR Study of CO_2 Capture by Butylamine and Oligopeptide KDDE in Aqueous Solution: Capture Efficiency and Gibbs Free Energy of the Capture Reaction as a Function of pH. *ChemPhysChem* **2023**, *24*, No. e202300053.

(23) Schell, J.; Yang, K.; Glaser, R. Computational Investigation of the Thermochemistry of the CO_2 Capture Reaction by Ethylamine, Propylamine, and Butylamine in Aqueous Solution Considering the Full Conformational Space via Boltzmann Statistics. *J. Phys. Chem. A* **2021**, *125*, 9578−9593.
(24) Gibbons, B. H.; Edsall, J. T. Rate of Hydration of Carbon Dioxide and Dehydration of Carbonic Acid at 25°. *J. Biol. Chem.* **1963**, *238*, 3502−3507.
(25) Harned, H. S.; Davis, R., Jr The Ionization Constant of Carbonic Acid in Water and the Solubility of Carbon Dioxide in Water and Aqueous Salt Solutions from 0 to 50°. *J. Am. Chem. Soc.* **1943**, *65*, 2030−2037.
(26) Dong, C.; He, G.; Zheng, W.; Bian, T.; Li, M.; Zhang, D. Study on antibacterial mechanism of $Mg(OH)_2$ nanoparticles. *Mater. Lett.* **2014**, *134*, 286−289.
(27) García-Río, L.; Hervés, P.; Leis, J. R.; Mejuto, J. C.; Rodríguez-Dafonte, P. Reactive micelles: nitroso group transfer from *N*-methyl-*N*-nitroso-*p*-toluenesulfonamide to amphiphilic amines. *J. Phys. Org. Chem.* **2004**, *17*, 1067−1072.
(28) King, J. F.; Gill, M. S.; Ciubotaru, P. Benzenesulfonyl chloride with primary and secondary amines in aqueous media - Unexpected high conversions to sulfonamides at high pH. *Can. J. Chem.* **2005**, *83*, 1525−1535.
(29) Ko, Y. G.; Shin, S. S.; Choi, U. S. Primary, secondary, and tertiary amines for CO_2 capture: Designing for mesoporous CO_2 adsorbents. *J. Colloid Interface Sci.* **2011**, *361*, 594−602.
(30) Puxty, G.; Rowland, R.; Allport, A.; Yang, Q.; Bown, M.; Burns, R.; Maeder, M.; Attalla, M. Carbon Dioxide Postcombustion Capture: A Novel Screening Study of the Carbon Dioxide Absorption Performance of 76 Amines. *Environ. Sci. Technol.* **2009**, *43*, 6427−6433.
(31) Rosman, K. J. R.; Taylor, P. D. P. Isotopic compositions of the elements 1997 (Technical Report). *Pure Appl. Geophys.* **1998**, *70*, 217−235.
(32) Jameson, B.; Glaser, R. Rotation-Inversion Isomerization of Tertiary Carbamates: Potential Energy Surface Analysis of Multi-Paths Isomerization Using Boltzmann Statistics. *ChemPhysChem* **2023**, *24*, 202200442.
(33) Pines, D.; Ditkovich, J.; Mukra, T.; Miller, Y.; Kiefer, P. M.; Daschakraborty, S.; Hynes, J. T.; Pines, E. How Acidic is Carbonic Acid? *J. Phys. Chem. B* **2016**, *120*, 2440−2451.
(34) Wang, X.; Conway, W.; Burns, R.; McCann, N.; Maeder, M. Comprehensive Study of the Hydration and Dehydration Reactions of Carbon Dioxide in Aqueous Solution. *J. Phys. Chem. A* **2010**, *114*, 1734−1740.
(35) Adcock, J. L. Teaching Bronsted−Lowry Acid−Base Theory in a Direct Comprehensive Way. *J. Chem. Educ.* **2001**, *78*, 1495−1496.
(36) Conrad, J.; Sasidharanpillai, S.; Tremaine, P. R. Second Dissociation Constant of Carbonic Acid in H_2O and D_2O from 150 to 325 °C at p = 21 MPa Using Raman Spectroscopy and a Sapphire-Windowed Flow Cell. *J. Phys. Chem. B.* **2020**, *124*, 2600−2617.
(37) Roughton, F. J. W. The Kinetics and Rapid Thermochemistry of Carbonic Acid. *J. Am. Chem. Soc.* **1941**, *63*, 2930−2934.
(38) Teranishi, K.; Ishikawa, A.; Sato, H.; Nakai, H. Systematic Investigation of the Thermodynamic Properties of Amine Solvents for CO_2 Chemical Absorption Using the Cluster-Continuum Model. *Bull. Chem. Soc. Japan.* **2017**, *90*, 451−460.
(39) Coe, J. V. Connecting cluster ions and bulk aqueous solvation: A new determination of bulk single ion solvation enthalpies. *Chem. Phys. Lett.* **1994**, *229*, 161−168.
(40) Tissandier, M. D.; Cowen, K. A.; Feng, W. Y.; Gundlach, E.; Cohen, M. H.; Earhart, A. D.; Coe, J. V.; Tuttle, T. R. The Proton's Absolute Aqueous Enthalpy and Gibbs Free Energy of Solvation from Cluster-Ion Solvation Data. *J. Phys. Chem. A* **1998**, *102*, 7787−7794.
(41) Kelly, C. P.; Cramer, C. J.; Truhlar, D. G. Aqueous Solvation Free Energies of Ions and Ion-Water Clusters Based on an Accurate Value for the Absolute Aqueous Solvation Free Energy of the Proton. *J. Phys. Chem. B* **2006**, *110*, 16066−16081.
(42) Zhan, C.-G.; Dixon, D. A. Absolute Hydration Free Energy of the Proton from First-Principles Electronic Structure Calculations. *J. Phys. Chem. A* **2001**, *105*, 11534−11540.
(43) Richard, R. M.; Bakr, B. W.; Sherrill, C. D. Understanding the Many-Body Basis Set Superposition Error: Beyond Boys and Bernardi. *J. Chem. Theory Comput.* **2018**, *14*, 2386−2400.
(44) Bachrach, S. M.; Streitwieser, A., Jr Electron Density Superposition Errors in Ethynyllithium. *J. Am. Chem. Soc.* **1984**, *106*, 2283−2287.
(45) Jameson, B.; Glaser, R. Unnatural Lysines with Reduced Sidechain *N*-Basicity: Synthesis of *N*-trifluoroethyl Substituted Lysine and Homologs. *ChemistrySelect* **2022**, *7*, No. e202203132.
(46) Jameson, B. *Investigation of Fluorinated CO2 Capture Systems*, Ph.D. Dissertation, Missouri University of Science and Technology: Rolla, MO, July 2023.
(47) Austin, A.; Petersson, G. A.; Frisch, M. J.; Dobek, F. J.; Scalmani, G.; Throssell, K. A density functional with spherical atom dispersion terms. *J. Chem. Theory Comput.* **2012**, *8*, 4989−5007.
(48) Becke, A. D. Density-functional thermochemistry. III. The role of exact exchange. *J. Chem. Phys.* **1993**, *98*, 5648−5652.
(49) Frisch, M. J.; Pople, J. A.; Binkley, J. S. Self-consistent molecular orbital methods 25. Supplementary functions for Gaussian basis sets. *J. Chem. Phys.* **1984**, *80*, 3265−3269.
(50) Marenich, A. V.; Cramer, C. J.; Truhlar, D. G. Universal Solvation Model Based on Solute Electron Density and on a Continuum Model of the Solvent Defined by the Bulk Dielectric Constant and Atomic Surface Tensions. *J. Phys. Chem. B.* **2009**, *113*, 6378−6396.
(51) *Gaussian 16, Revision C.01*, Frisch, M. J.; Trucks, G. W.; Schlegel, H. B.; Scuseria, G. E.; Robb, M. A.; Cheeseman, J. R.; Scalmani, G.; Barone, V.; Petersson, G. A.; Nakatsuji, H.; Li, X.; Caricato, M.; Marenich, A. V.; Bloino, J.; Janesko, B. G.; Gomperts, R.; Mennucci, B.; Hratchian, H. P.; Ortiz, J. V.; Izmaylov, A. F.; Sonnenberg, J. L.; Williams-Young, D.; Ding, F.; Lipparini, F.; Egidi, F.; Goings, J.; Peng, B.; Petrone, A.; Henderson, T.; Ranasinghe, D.; Zakrzewski, V. G.; Gao, J.; Rega, N.; Zheng, G.; Liang, W.; Hada, M.; Ehara, M.; Toyota, K.; Fukuda, R.; Hasegawa, J.; Ishida, M.; Nakajima, T.; Honda, Y.; Kitao, O.; Nakai, H.; Vreven, T.; Throssell, K.; Montgomery, J. A., Jr.; Peralta, J. E.; Ogliaro, F.; Bearpark, M. J.; Heyd, J. J.; Brothers, E. N.; Kudin, K. N.; Staroverov, V. N.; Keith, T. A.; Kobayashi, R.; Normand, J.; Raghavachari, K.; Rendell, A. P.; Burant, J. C.; Iyengar, S. S.; Tomasi, J.; Cossi, M.; Millam, J. M.; Klene, M.; Adamo, C.; Cammi, R.; Ochterski, J. W.; Martin, R. L.; Morokuma, K.; Farkas, O.; Foresman, J. B.; Fox, D. J. Gaussian, Inc.: Wallingford CT, 2016.
(52) McKay, R. T. How the 1D-NOESY suppresses solvent signal in metabonomics NMR spectroscopy: An examination of the pulse sequence components and evolution. *Concepts Magn. Reson., Part A* **2011**, *38A*, 197−220.
(53) Vanzijl, P. C. M.; Sukumar, S.; Johnson, M. O.; Webb, P.; Hurd, R. E. Optimized Shimming for High-Resolution NMR Using Three-Dimensional Image-Based Field Mapping. *J. Magn. Reson., Ser. A* **1994**, *111*, 203−207.

https://doi.org/10.1021/acs.joc.3c00701
J. Org. Chem. 2023, 88, 11534−11544